Absorption and Emission Spectra in Aqueous Solution with Coupled-Cluster Accuracy

Niklas Sülzner,[a] Ömer F. C. Tiska,[a] Julia Haberhauer,[a] Patrick Kibies,[b] Stefan M. Kast,[b] Christof Hättig,*[a]

Quantitative prediction of electronic spectra in water requires an accurate treatment of electronic excitation, nuclear structure, and state-specific solvation including effects from hydrogen bonding. Here, photoacids and photobases in aqueous solution are used as stringent test systems for a novel workflow combining state-specific embedded cluster reference interaction site model calculations combined with the iterative coupled cluster models CC2 and CC3, and complementary Wigner nuclear-ensemble and adiabatic Hessian Franck-Condon treatments for spectral simulation. This combination reproduces without empirical shift or scaling corrections absorption and emission band maxima on an absolute energy scale with typical errors of only 0.1–0.2 eV. The energies of resolved 0–0 transitions in photobases are reproduced even more accurately, within a few hundredths of an eV. The simulations also resolve contributions from different excited states and changes in the emitting species. Derived excited-state acidity changes, $\Delta \mathrm{p}K_\mathrm{a}^*$, show similar accuracy for photoacids and photobases, with residual errors governed by cancellation or accumulation between protonation states. The computational costs of this workflow are low enough to make it suitable for routine applications to aromatic chromophores with up to three rings.

Introduction

Electronic absorption and fluorescence spectra are among the most important experimental probes of electronically excited states and their interaction with an environment. Their quantitative prediction with electronic and molecular structure calculations, however, remains challenging. This is in particular the case in aqueous solution, where hydrogen-bonding interactions with the solvent are responsible for shifts in transition energies that depend largely on the protonation state and the electronic character of a transition. Experimental spectra reflect not only the electronic transition energies, but also nuclear motion, vibronic coupling, thermal fluctuations, and solvation.[1] Consequently, vertical excitation energies, 0–0 transition energies, and spectral band maxima represent distinct quantities that can differ considerably.[2] Predicting spectral band profiles therefore provides a substantially more stringent test of an excited-state description than comparison with isolated transition energies, since band positions, shapes, vibronic structure, and electronic-state contributions have to be reproduced simultaneously.

Modern Franck–Condon and Herzberg–Teller approaches provide access to vibrationally resolved absorption and fluorescence spectra,[3,4] and have enabled direct simulations of spectral line shapes in solution.[5] For molecules in solution, this task is complicated by the large number of nuclear and solvent degrees of freedom. Explicit configurational sampling naturally accounts for thermal fluctuations, conformational flexibility, and heterogeneous solvent environments, whereas quantum-mechanical vibronic treatments provide a detailed description of the intramolecular nuclear degrees of freedom.[1,6] Both aspects are particularly important in water, where directional hydrogen bonding and solvent reorganization are strongly coupled to excitation-induced changes in the electronic charge distribution. Accordingly, different strategies have been developed to combine nuclear ensemble sampling and vibronic spectroscopy.[7–10] Their application together with accurate electronic-structure methods remains computationally demanding, however, and practical calculations therefore involve a compromise between configurational sampling and the accuracy of the underlying excitation energies.[11] As a consequence, calculated spectra are often shifted or aligned with experimental reference data when the emphasis is placed primarily on band shapes or solvent effects.[12,13] Recent calculations have demonstrated that predictive aqueous absorption spectra without such empirical adjustments are becoming accessible, including path-integral molecular dynamics sampling combined with ADC(2) for indole[14] and multiconfigurational calculations in polarizable atomistic environments for benzene and phenol.[15] Related recent strategies employ machine learning to transfer high-level electronic-structure information to condensed-phase ensembles or to construct physically decomposed environmental spectral densities,[11,16] while nonadiabatic coupling between closely spaced electronic states has recently been shown to affect solution-phase absorption line shapes of indole derivatives.[17] Huge computational costs, however, hamper the application of these methods to more than very few show cases. Also, quantitative calculations that simultaneously address absorption and fluorescence or 0–0 transitions in water are considerably less established.[13–15,17,18]

Fluorescence poses an additional challenge because both the molecular structure and the slow nuclear and orientational components of the solvent polarization respond to the excited-state charge distribution before emission, whereas

[a] Dr. N. Sülzner, Ö. F. C. Tiska, J. Haberhauer, Prof. Dr. C. Hättig*
Lehrstuhl für Theoretische Chemie
Ruhr-Universität Bochum
44780 Bochum, Germany
E-mail: christof.haettig@rub.de

[b] Dr. P. Kibies, Prof. Dr. S. M. Kast
Fakultät für Chemie und Chemische Biologie
Technische Universität Dortmund
Otto-Hahn-Straße 4a
44227 Dortmund, Germany

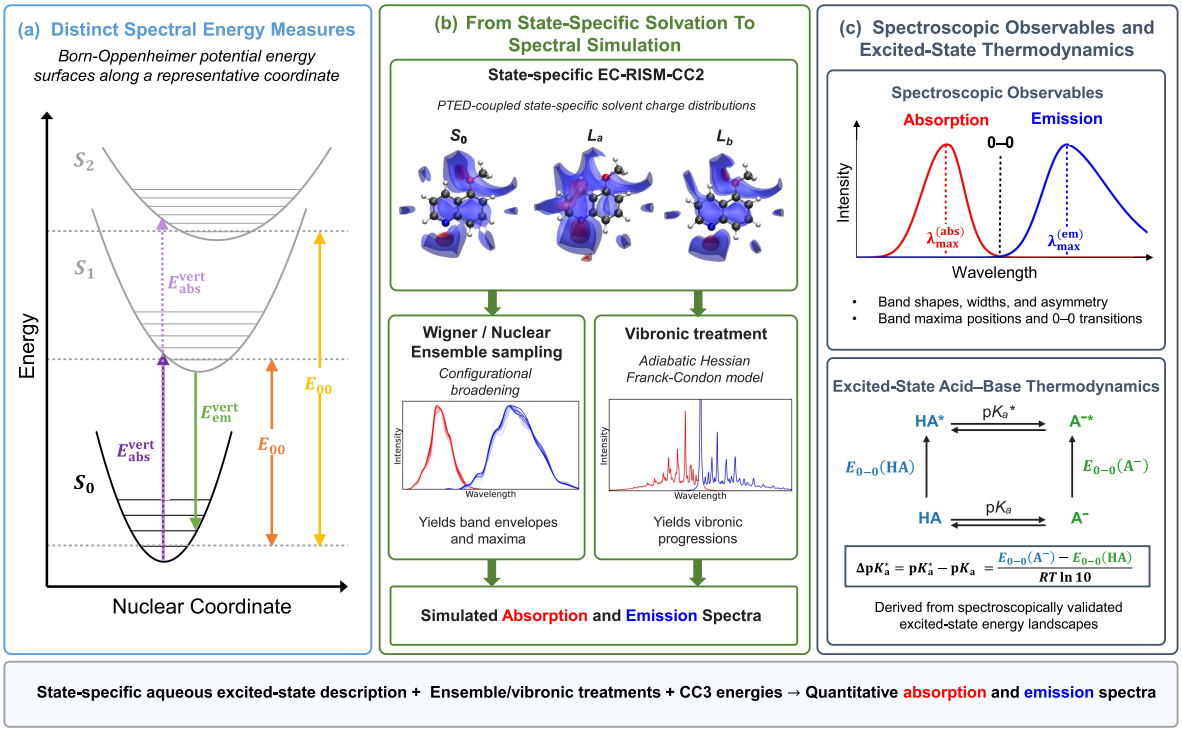


Figure 1. Conceptual overview of the computational strategy used to connect aqueous excited-state electronic structure with experimental spectral observables and excited-state acid-base thermodynamics. (a) Schematic distinction between vertical absorption/emission energies and 0–0 transition energies. (b) State-specific EC-RISM-CC2 calculations employing the PTED coupling scheme in combination with CC3 energies provide the basis for two complementary routes: nuclear-ensemble approach (NEA) for band envelopes and maxima, and adiabatic Hessian Franck-Condon (AHFC) calculations for vibronic structure and spectral origins. (c) The resulting absorption and fluorescence spectra are compared directly with experiment, while protonation-state-dependent excited-state energies provide access to $\Delta \mathrm{p}K_\mathrm{a}^*$.

the optical transition itself induces a fast, nonequilibrium response of the electronic charge distribution of the environment. A consistent treatment therefore requires accurate excited-state structures and energies together with a state-specific description of solvation.[19,20] An alternative to the large computational burden of explicit solvent sampling is provided by statistical-mechanical solvation models.[21] In particular, the embedded-cluster reference interactions site model[22,23] (EC-RISM) retains atomically resolved solvent site distributions and can therefore describe solvent granularity and directional solute–solvent interactions while remaining compatible with correlated wave-function methods.[21,22] A recent implementation[24] of ground- and excited-state gradients for EC-RISM combined with the approximate coupled-cluster singles and doubles model CC2[25] enables the solvent distribution to be equilibrated self-consistently with the respective electronic state. For the separation into fast (electronic) and slow (nuclear) contributions, EC-RISM is combined with the conductor-like screening model[26,27] (COSMO) to account for the linear response and non-equilibrium contributions to electronic transitions which involve only the fast component of the solvent response.[19,20,24]

Here, we apply this framework to aqueous solutions of photoacids and photobases as particularly demanding test systems with different protonation states for quantitative excited-state spectroscopy.[28,29] Protonation and deprotonation produce pronounced changes in electronic structure and hydrogen bonding, while several of the compounds additionally exhibit closely spaced L_a and L_b states with overlapping spectral contributions but different polarity, or changes in the identity of the emitting species.[30,31] Previous calculations demonstrated that the solvent granularity provided by EC-RISM is particularly important for the deprotonated photoacids.[32]

The current work applies for the first time a workflow that combines state-specific EC-RISM-CC2 calculations employing the PTED coupling scheme with the iterative approximate triples model CC3[33] and two complementary spectral treatments: a nuclear ensemble approach (NEA)[34] with Wigner distributions and adiabatic Hessian Franck-Condon (AHFC) calculations.[3,4] The resulting absorption and fluorescence spectra are compared directly without shifting with experiment on an absolute energy scale, allowing the accuracy of band positions, state-specific spectral contributions, and 0–0 energies to be assessed. Finally, the spectroscopically benchmarked excitation energies are used to determine $\Delta \mathrm{p}K_\mathrm{a}^*$, probing how residual excitation-energy errors of the corresponding protonation states cancel or accumulate when excited-state acid–base thermodynamics is derived.

Results and Discussion

From Vertical Excitations to Absorption and Fluorescence Spectra in Water

The conceptual approach used in this work to simulate state-resolved absorption and fluorescence spectra is summarized in Fig. 1. Spectroscopic observables of particular interest are the band maxima, E_max, and the 0–0 transition energies, E_{00}. The latter correspond to the energy difference

between the vibrational ground levels associated with the relaxed ground- and excited-state minima and therefore include the difference in zero-point vibrational energies. In contrast, the positions and shapes of absorption and fluorescence bands depend on the nuclear-coordinate distribution and vibronic structure. Consequently, their maxima $E_{\max}$ generally differ from the corresponding vertical transition energies E_{vert}, which are evaluated at a single nuclear geometry.

The systems considered in this work comprise aqueous photoacids and photobases (see Fig. S1, SI). For each system, we considered the electronically excited states contributing to the lowest-energy UV/Vis absorption band and to the fluorescence spectrum. In many cases, these correspond to the two lowest $\pi\pi^*$ states, which can generally be assigned L_a and L_b character according to Platt's notation.[28,35] Depending on the molecular system, either one or both of these states contribute to the experimentally observed spectra.

A quantitative description of $E_{\max}$ and E_{00} in aqueous solution requires (i) an accurate electronic-structure treatment, (ii) an appropriate description of the state-specific solvent response, and (iii) a treatment of the nuclear degrees of freedom. Here, excited-state structures are obtained using EC-RISM-CC2 calculations employing the state-specific PTED coupling scheme. This allows the solvent distribution to equilibrate self-consistently with the respective ground or excited electronic state. Excitation energies have been calculated with the approximate coupled cluster singles, doubles, and triples model CC3 using the structures and solvent potentials optimized at the CC2 level.

The vibrational contributions to the spectra are accounted for using two complementary methods: a nuclear ensemble approach (NEA) with Wigner distributions and adiabatic Hessian Franck-Condon (AHFC) calculations. The NEA approach provides band envelopes and maxima, whereas the AHFC treatment resolves the vibronic progression and spectral structure. Both approaches therefore yield simulated absorption and fluorescence spectra whose band positions and shapes can be compared directly with experiment.

For a consistent comparison of experimental and calculated band positions, the relevant absorption and fluorescence bands were analyzed by fitting suitable line-shape functions rather than by taking the maxima of the raw spectra directly. Where required, overlapping contributions from different electronic states or protonation states, as well as distinct 0–0 features, were deconvoluted before assigning the corresponding band maxima. The resulting fitted band maxima are used throughout the quantitative comparisons and error statistics; details of the fitting procedures and molecule-specific choices are provided in the Supporting Information.

Finally, differences between the excited-state energies of conjugate acid–base forms provide access to the corresponding changes in acidity or basicity, quantified by $\Delta \mathrm{p}K_{\mathrm{a}}^{*}$. These quantities provide an additional test of how residual excitation-energy errors for absorption and emission in the two protonation states cancel or accumulate when energy differences are formed. Having established how the different calculated energy measures map onto experimental spectral observables, we first consider the chemically more heterogeneous photoacid series.

Spectral Signatures of Photoacids in Aqueous Solution

2-Naphthol (2NOH) is selected as the prime example, with its spectra shown in Fig. 2 (left). For this photoacid, L_b is the relevant state for both absorption and emission of the neutral species, 2NOH (Fig. 2(a)), as well as of the deprotonated anionic species, $2\mathrm{NO}^-$ (Fig. 2(b)); $S_2(L_a)$ does not contribute to the emission and the lowest absorption bands. In general, the calculated NEA and AHFC spectra reproduce the experimental band shapes well, although distinct differences are found for the positions of the band maxima, $E_{\max}$.

The experimental absorption spectrum of 2NOH exhibits a pronounced low-energy feature assigned to the 0–0 transition, which constitutes the maximum of the full spectrum.[37] To obtain a characteristic maximum for the remaining broad vibronic contribution, the experimental spectrum was therefore decomposed into two Gaussian components, yielding a maximum of 3.91 eV for the latter. The calculated maxima bracket this value: The NEA maximum at 3.98 eV is blue-shifted by 0.07 eV, whereas the AHFC maximum at 3.87 eV lies 0.03 eV lower in energy. The latter comparison should be regarded as approximate because the experimental and calculated vibronic spectra do not permit an entirely analogous decomposition. Both calculated spectra nevertheless reproduce the overall position and shape of the broad absorption envelope well. The calculated theoretical best estimate (TBE) of $E_{00} = 3.76$ eV agrees very well with the value $E_{00}^{\mathrm{expl}} = 3.75$ eV obtained from the Gaussian deconvolution of the experimental absorption spectrum. Both values are close to the independent experimental absorption–emission midpoint estimate of $E_{00}^{\mathrm{exptl,mid}} = 3.72$ eV. For fluorescence, the NEA spectrum reproduces the experimental band maximum almost quantitatively, with 3.55 eV compared with 3.54 eV experimentally, corresponding to a deviation of only 0.01 eV. The AHFC maximum of 3.63 eV is moderately blue-shifted by 0.09 eV.

For $2\mathrm{NO}^-$, the dependence of the calculated band maximum on the simulation appraoch for the specta is more pronounced. The experimental absorption maximum of 3.57 eV is reproduced closely by the AHFC spectrum at 3.55 eV (-0.02 eV), whereas the NEA maximum at 3.79 eV is blue-shifted by 0.22 eV. The opposite behavior is observed for fluorescence: relative to the experimental maximum at 2.99 eV, the AHFC treatment gives a pronounced blue shift to 3.25 eV ($+0.26$ eV), whereas the NEA maximum at 2.85 eV is red-shifted by 0.14 eV. The TBE for the 0–0 transition is 3.39 eV, compared with an experimental midpoint estimate of 3.28 eV. The complete experimental and calculated band maxima of all studied photoacids are compiled in Tab. S1; the corresponding deviations between theoretical and experimental values are shown in Fig. S2 of the Supporting Information (SI).

Already for this representative example, a systematic difference between the two spectral treatments becomes apparent. For absorption, the NEA band maxima tend to be blue shifted, whereas the band maxima from the AHFC calculations appear at lower energies. For fluorescence, these trends are reversed, with the NEA maxima shifted toward lower and the AHFC maxima toward higher energies. The essentially vanishing error of the NEA distribution for the fluorescence maximum of neutral 2NOH represents an exception in magnitude, but not a significant contradiction

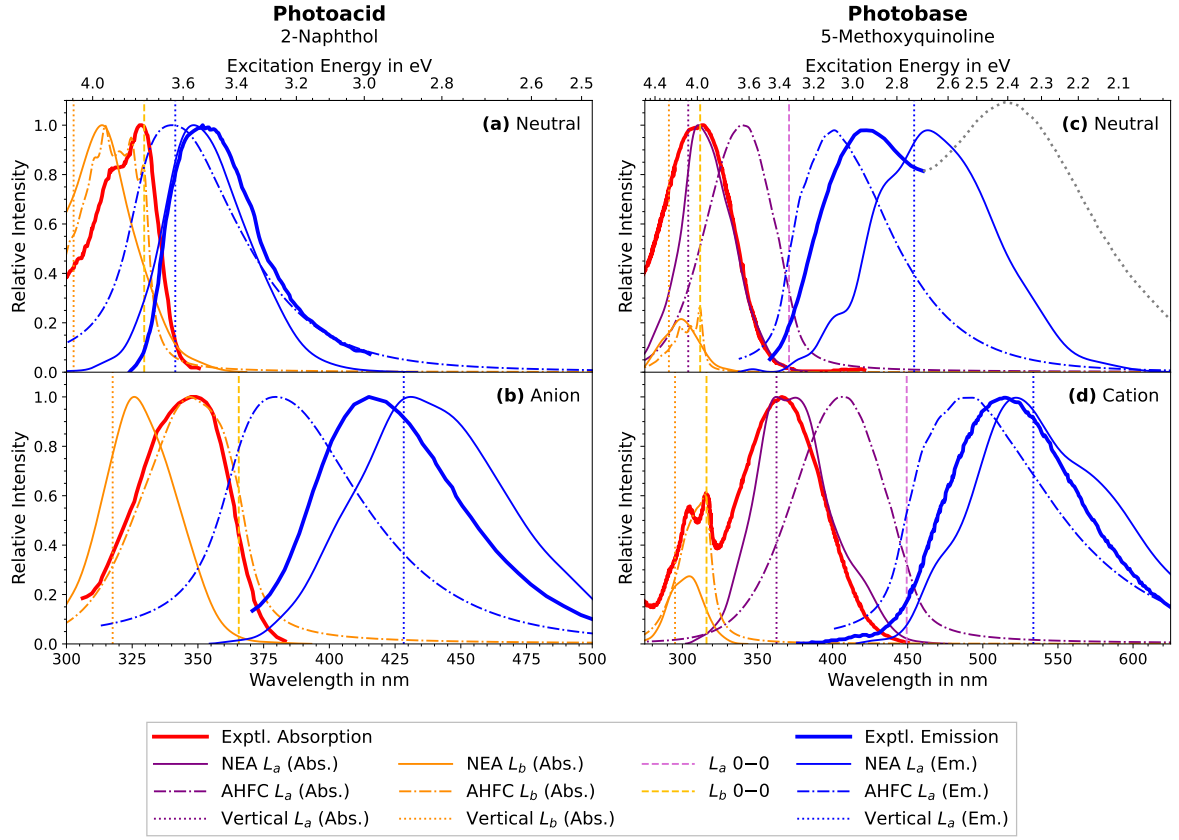


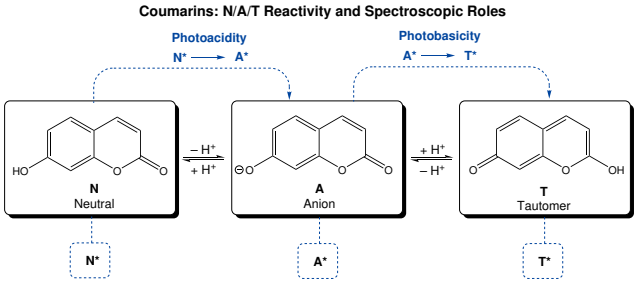
Figure 2. Simulated and experimental spectra of the photoacid 2-naphthol (left) and the photobase 5-methoxyquinoline (right) as representative examples. Neutral species (top) and corresponding deprotonated or protonated species (bottom), respectively. Experimental absorption and fluorescence spectra are shown in, respectively red and blue; Calculated NEA and AHFC spectra, vertical transition energies, and 0–0 energies are shown for the corresponding L_a and L_b states as indicated in the legend. Experimental spectra of 2-naphthol and 2-naphtholate were taken from Refs. 36,37, respectively; the experimental 5-methoxyquinoline spectra were taken from Ref. 38.

to this overall trend. These opposing trends in the errors of NEA and AHFC calculations are a consequence of very different approximations used in these approaches to simulate the band structure: While NEA calculations include the full anharmonicity of the ground- and excited-state potential energy surfaces, they have no information on the excited-state equilibrium geometry and vibrational frequencies. The AHFC calculations, on the other hand, account for the changes in the equilibrium structure and vibrational frequencies from the ground- to the excited state, but use the harmonic approximation. Whether these trends persists across the chemically broader benchmark will be examined below for the photobases and subsequently quantified for the complete data set.

Another characteristic feature of the 2NOH/2NO$^-$ spectra is the approximate mirror symmetry between absorption and fluorescence. When normalized to the same maximum intensity and represented on an energy scale, the two bands exhibit similar shapes on opposite sides of their overlap region. This behavior is consistent with the well-known mirror-image rule, which is expected when absorption and fluorescence connect the same pair of electronic states and the vibrational normal modes and potential-energy-surface curvatures of the two states remain sufficiently similar.[4,39] Under these idealized conditions, the symmetry center of the absorption and fluorescence profiles lies close to the 0–0 transition energy. For 2NO$^-$ in particular, the intersection region of the calculated vibronic absorption and fluorescence spectra agrees closely with the calculated 0–0 energy.

Beyond 2-naphthol, the remaining photoacids probe several additional challenges for the spectral simulations, including closely spaced electronic states, changes in the state ordering between vertical and 0–0 transitions, and changes in the identity of the emitting species. One such aspect is the electronic-state character. For the studied phenols, except 4-cyanophenol (4CNPhOH), the lowest relevant excited state is $S_1(L_b)$, which lies more than ≈ 1 eV below $S_2(L_a)$. For 4CNPhOH, the L_a and L_b states are considerably closer in energy and both contribute to the absorption spectrum, with the more intense higher-energy band associated with $S_2(L_a)$, whereas fluorescence originates from $S_1(L_b)$.[32,40] Despite the close-lying absorption bands, their positions are reproduced well: the NEA maxima deviate from experiment by 0.06 and 0.14 eV for L_b and L_a, respectively, while the AHFC L_b maximum differs by only 0.05 eV. The calculated L_b fluorescence maximum is blue-shifted by 0.14 eV with both spectral treatments. For 1-naphthol (1NOH) and 1NO$^-$, the L_a and L_b states are likewise close in energy and their absorption bands strongly overlap, in line with experiment[41–43]. For neutral 1NOH, only an L_a excited-state minimum could be optimized, precluding a comparison of the relative adiabatic energies of separate L_a and L_b minima. Experimentally, a distinct L_b 0–0 feature can nevertheless be identified for 1NOH, whereas the remaining broad

absorption envelope cannot be unambiguously decomposed into separate L_a and L_b contributions. For $1NO^-$, the overlapping absorption contributions likewise prevent an unambiguous state-resolved experimental assignment. 5-Cyano-2-naphthol (5CN2NOH) further illustrates the sensitivity of the relative L_a/L_b energies to substitution: In contrast to 2NOH, cyano substitution stabilizes L_a sufficiently to become the lower of the two states, analogous to the ordering found for 5CN1NOH. [32,44]



Scheme 1. Acid–base and tautomeric relationships of the hydroxycoumarins considered in this work. The neutral form **N**, anion **A**, and tautomer **T** are connected through proton-transfer equilibria. In the excited state, deprotonation of **N*** corresponds to photoacidity, whereas protonation of **A*** can lead to the tautomeric form **T***, representing the complementary photobasic pathway.

Lastly, the hydroxycoumarins provide a qualitatively different challenge because their excited-state proton-transfer pathways can lead to an emitting species that differs from the initially excited neutral form (Scheme 1). For 7-hydroxycoumarin and 4-methyl-7-hydroxycoumarin, the calculated L_a absorption bands of the neutral forms reproduce the experimental spectra in aqueous solution closely. Their fluorescence spectra contain two contributions that can be approximately separated into a small higher-energy band with small intensity assigned to the emission from the neutral form and a dominant lower-energy band with high intensity assigned to the tautomeric form. [45–47] The relative TBEs for the total energies in solution including solvation energy and the zero-point vibrational (ZPV) contributions support this assignment. For 7-hydroxycoumarin and 4-methyl-7-hydroxycoumarin, tautomerization is endothermic by 71 and 68 kJ mol^{-1}, respectively, in the ground state, but exothermic by 10 and 11 kJ mol^{-1} in the S_1 state. Thus, the calculations are consistent with a thermodynamic equilibrium in S_0 where essentially only the normal neutral form exists, whereas in S_1 the tautomer is strongly favored and the normal form is expected to contribute only at the percent level. The AHFC spectra reproduce the energetic separation of these two emission components well, particularly for 4-methyl-7-hydroxycoumarin: the experimental neutral–tautomer separations of 0.58 and 0.31 eV for 7-hydroxycoumarin and 4-methyl-7-hydroxycoumarin, respectively, are calculated as 0.71 and 0.33 eV. The corresponding NEA spectra predict larger separations of 0.87 and 0.88 eV. The spectral simulations therefore provide information not only on band positions but also on the identity of the emitting species. For 3-hydroxycoumarin, the fluorescence spectrum contains only one band which is assigned to an emission from S_1 of the normal neutral from of 3-hydroxycoumarin. In agreement with these observations, the tautomerization energies obtained for 3-hydroxycoumarin from the TBEs for the total energies in solution including solvation energy and ZPV contributions in S_0 and S_1 are, respectively, +71 and +19 kJ/mol, i.e. the tautomerization equilibrium remains for 3-hydroxycoumarin in S_1 practically completely on the side of the normal neutral form.

State-Resolved Spectroscopy of Photobases in Aqueous Solution

In contrast to the photoacids, the spectral simulations for the photobases do more than reproduce the overall spectral positions: they resolve the electronic-state composition of the experimental spectra. As a representative example, we consider 5-methoxyquinoline (5MeOQ), whose neutral and protonated spectra are shown in Fig. 2(c,d).

Both L_a and L_b contribute to the absorption spectra of neutral 5MeOQ and its protonated form, $5MeOQH^+$, whereas fluorescence originates from the lower-lying L_a state only. [48] As above for 2NOH and $2NO^-$, the calculated spectra generally reproduce the experimental spectral profiles well, although pronounced differences between the NEA and AHFC treatments are found for some band maxima. For neutral 5MeOQ, the experimental L_a absorption maximum at 4.02 eV is reproduced at 3.93 eV by the NEA spectrum, corresponding to a moderate red shift of 0.09 eV. The AHFC spectrum is considerably further red-shifted, with a maximum at 3.67 eV (−0.36 eV). The calculated L_b absorption is substantially weaker and is therefore largely superimposed on the dominant L_a absorption in the spectrum of 5MeOQ. Consequently, a separate experimental band maximum for the vibronic L_b contribution cannot be determined reliably. Its experimentally resolved 0–0 origin is considered separately below.

For fluorescence, the same opposing trends of the two spectral treatments are found as already observed above for the photoacid example. For neutral 5MeOQ, the NEA maximum at 2.67 eV is red-shifted by 0.31 eV relative to experiment (2.96 eV), whereas the AHFC maximum at 3.11 eV is blue-shifted by 0.15 eV. For $5MeOQH^+$, the corresponding deviations are substantially smaller for the NEA treatment: the experimental maximum of 2.42 eV is well reproduced with 2.36 eV (−0.06 eV), while the AHFC spectrum has its maximum at 2.55 eV, blue-shifted by 0.13 eV. The apparently larger widths of these fluorescence bands when displayed on a wavelength scale should not by themselves be interpreted as stronger physical broadening, since a given energy interval spans an increasingly large wavelength range toward lower transition energies.

A particularly characteristic feature of the photobase absorption spectra is provided by the higher-lying L_b state. This is especially apparent for $5MeOQH^+$: although the spectrum is dominated by L_a, the weaker L_b contribution is clearly resolved in the high-energy region. The corresponding NEA band maximum of 4.10 eV differs by only 0.01 eV from the experimental maximum at 4.09 eV, while the maximum of the AHFC spectrum at 4.04 eV remains within 0.05 eV. Even more striking is the agreement of the directly resolved L_b 0–0 origin. For neutral 5MeOQ, the experimental origin at 3.96 eV is reproduced at 3.98 eV by the calculated TBE. [48] For $5MeOQH^+$, the TBE of 3.92 eV differs by only ∼0.01 eV from the experimental origin at 3.93 eV. As shown below, this exceptionally close agreement is not restricted to 5MeOQ but is characteristic of the photobase L_b 0–0 energies across the benchmark and reflects the accuracy of the electronic and molecular structure approach

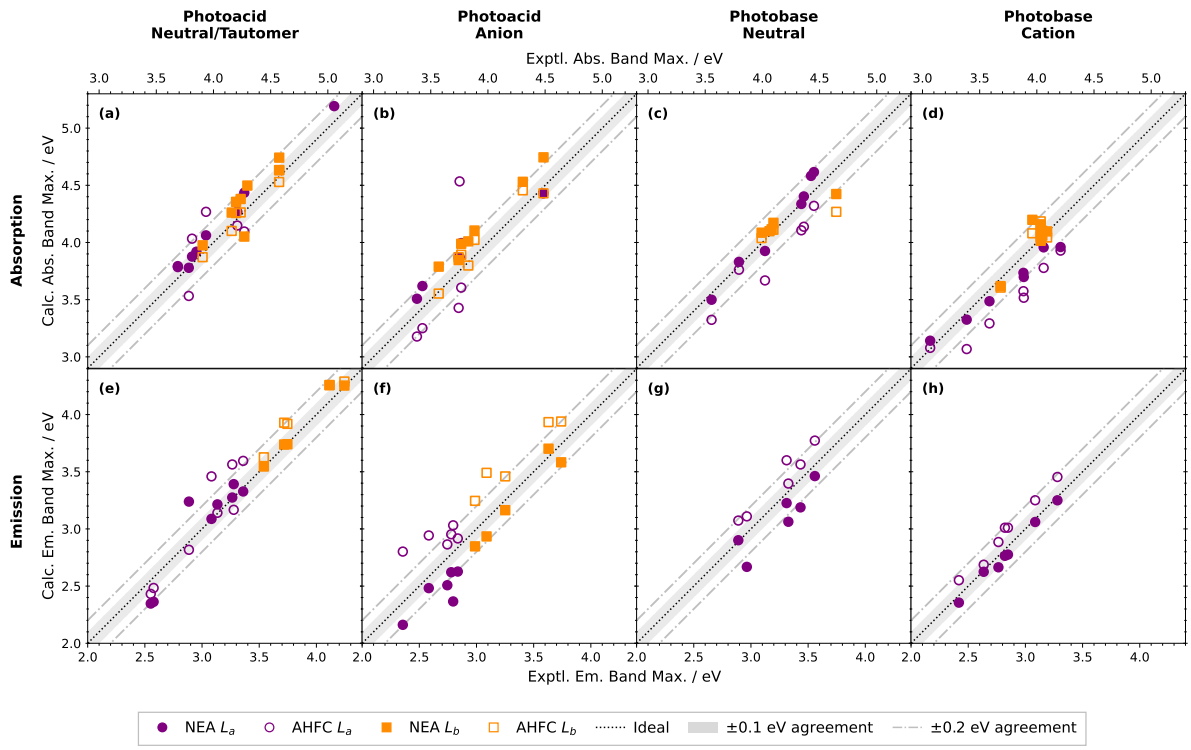


Figure 3. Comparison of calculated and experimental absorption (top row) and emission (bottom row) band maxima for aqueous photoacids and photobases. Photoacids are shown separately for neutral (incl. tautomeric) (a,e) and anionic forms (b,f); photobases for neutral (c,g) and cationic (d,h) forms. The dotted diagonal indicates perfect agreement between calculation and experiment; the shaded region marks deviations within ±0.10 eV of the ideal relation. Corresponding error statistics are given in Tab. 1.

and the unambiguous assignment of the 0–0 transitions in the experimental spectra.

As for the 2NOH/2NO$^-$ example, the L_a absorption and fluorescence profiles of 5MeOQ and 5MeOQH$^+$ also exhibit approximate mirror-image behavior. Consistent with this picture, the L_a 0–0 midpoint estimates obtained from the calculated absorption and fluorescence maxima lie close to the directly calculated TBE values for the 0–0 transition energies. For neutral 5MeOQ, the AHFC and NEA midpoint estimates are 3.39 and 3.30 eV, respectively, compared with a TBE of 3.34 eV and an experimental midpoint estimate of 3.49 eV. For 5MeOQH$^+$, the corresponding calculated midpoint estimates are 2.81 and 2.84 eV, compared with a TBE of 2.76 eV and an experimental midpoint estimate of 2.90 eV. Thus, all three calculated L_a 0–0 measures are somewhat lower than the experimental midpoint estimates, with deviations remaining within approximately 0.20 eV for both protonation states.

The remaining photobases show the same general state-resolved picture, although the available spectroscopic information and calculated vibronic structure are not equally complete for every compound.[48] Acridine provides the notable additional case of a directly resolved L_a 0–0 origin. A complete account of the available band maxima and state-specific data coverage of the photobases is provided in Tab. S2, with the corresponding deviations between computational and experimental values are shown in Fig. S3 of the SI.

Quantitative Accuracy Across Absorption, Emission, and 0–0 Energies

An overview of the statistical analysis of the band maxima from the NEA and AHFC calculations with respect to experiment is provided by the correlation plots in Fig. 3 and the corresponding error statistics in Tab. 1. The data are resolved according to photoacids and photobases, neutral and ionic species, absorption and fluorescence, the NEA and AHFC treatments, and, where applicable, the L_a and L_b states. In Tab. 1, the available L_a and L_b bands of the photoacids are treated jointly, whereas for the photobase these states are reported separatedly since they exhibit different trends. Detailed molecule-resolved band maxima are provided in Tabs. S1–S2, with the corresponding signed errors shown in Figs. S2–S3. Error statistics are given in Tabs. S3–S4.

As can be seen in Fig. 3, most of the calculated band maxima lie within ±0.2 eV of experiment, and many fall within the ±0.1 eV interval. The correlation diagrams also reveal systematic differences between the NEA and AHFC spectral simulations. For photoacid absorption, the NEA maxima show a systematic tendency toward higher energies, with mean deviations of +0.09 and +0.17 eV for the neutral and anionic subsets, respectively (Tab. 1). The corresponding MADs are 0.12 and 0.18 eV. In contrast, the AHFC mean deviations are close to zero, at +0.02 eV for the neutral species and +0.03 eV for the anions. However, the corresponding MADs of 0.12 and 0.19 eV are comparable to, and slightly larger than, the NEA values, showing that the small signed deviations partly result from cancellation of positive and negative individual deviations.

Table 1. Error statistics (in eV) for calculated absorption and emission band maxima and photobase L_b 0–0 energies relative to experiment. For the band maxima, results from the nuclear ensemble approach (NEA) are given first and results from the adiabatic hessian Franck-Condon (AHFC) calculations in parentheses. Photobase L_b 0–0 energies are compared with directly calculated TBE values.

Systems	Observable	Species	State	N[a]	MD[b]	MAD[c]	MaxAE[d]
Photoacids	Abs. Max.	Neutral[e]	Combined[f]	16 (12)	0.087 (0.015)	0.115 (0.119)	0.218 (0.333)
		Anion	Combined[f]	13 (12)	0.167 (0.031)	0.175 (0.190)	0.258 (0.782)
	Em. Max.	Neutral[e]	Combined[f]	13 (13)	0.022 (0.091)	0.092 (0.151)	0.354 (0.377)
		Anion	Combined[f]	11 (11)	−0.163 (0.253)	0.176 (0.253)	0.430 (0.446)
Photobases	Abs. Max.	Neutral	L_a	7 (6)	0.034 (−0.202)	0.079 (0.202)	0.165 (0.355)
		Neutral	L_b	5 (3)	0.003 (−0.106)	0.092 (0.146)	0.222 (0.378)
		Cation	L_a	7 (7)	−0.110 (−0.263)	0.131 (0.266)	0.248 (0.369)
		Cation	L_b	7 (7)	0.057 (0.038)	0.081 (0.074)	0.238 (0.151)
	Em. Max.	Neutral	L_a	6 (6)	−0.163 (0.172)	0.167 (0.172)	0.296 (0.288)
		Cation	L_a	7 (7)	−0.051 (0.143)	0.051 (0.143)	0.100 (0.190)
	0–0 Transition	Neutral	L_b	4	0.018	0.018	0.030
		Cation	L_b	6	0.019	0.021	0.056

[a] N: Number of available experimental comparisons.
[b] MD: mean (signed) deviation. [c] MAD: mean absolute deviation. [d] MaxAE: maximum absolute error.
[e] Neutral normal and tautomeric photoacid forms are combined.
[f] Available L_a and L_b photoacid bands are treated jointly.

For fluorescence, the clearest reversal between the two spectral treatments is found for the anionic photoacids. The NEA maxima are shifted toward lower energies on average [Mean deviation (MD) = −0.17 eV; Mean absolute deviation (MAD) = 0.18 eV], whereas the AHFC maxima are shifted toward higher energies (MD = +0.25 eV, MAD = 0.25 eV). For the neutral species, both mean deviations are positive but substantially smaller, with MDs of +0.04 and +0.10 eV and MADs of 0.11 and 0.16 eV for NEA and AHFC, respectively. The somewhat larger absolute deviations found for the anionic species, particularly in fluorescence, are consistent with their more demanding solvation environment, for which directional hydrogen-bond donation by water and the state-specific solvent response become especially important.

Across the photoacid set, no clear systematic dependence of the deviations on L_a or L_b character is apparent. Instead, the dominant trends are associated with the spectral treatment and protonation state, consistent with the behavior already observed for the representative 2NOH/2NO$^-$ example.

A similar picture emerges for the photobases, although both L_a and L_b contribute to the absorption spectra. For the neutral species, the NEA maxima show only small positive mean deviations of +0.03 eV for L_a and +0.00 eV for L_b, with MADs of 0.08 and 0.09 eV, respectively. The corresponding AHFC maxima are shifted to lower energies on average, with mean deviations of −0.20 eV for L_a and −0.11 eV for L_b, and MADs of 0.20 and 0.15 eV, respectively. For the cationic species, the situation is less uniform. Both treatments underestimate the L_a absorption maxima on average (MD = −0.11 and −0.26 eV for Wigner and AHFC spectra, respectively), whereas the L_b maxima show small positive mean deviations of +0.06 and +0.04 eV. Thus, the cationic absorption bands constitute one of the cases for which the two treatments do not bracket experiment systematically.

For the photobase fluorescence maxima, the opposing shifts in the NEA and AHFC results are recovered clearly. For the neutral species, the mean deviations are −0.16 and +0.17 eV, with MADs of 0.17 and 0.17 eV, respectively. For the cations, the NEA treatment performs particularly well,

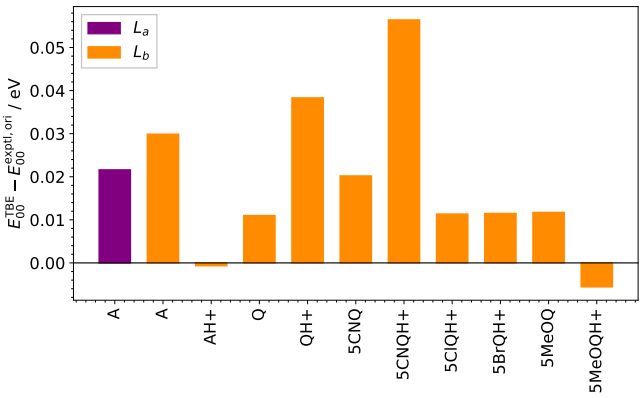


Figure 4. Signed deviations of calculated photobase 0–0 transition energies from experimentally resolved spectral origins. The errors are defined as $E_{00}^{\mathrm{TBE}} - E_{00}^{\mathrm{exptl,ori}}$. Corresponding statistical errors for the L_b subset are given in Tab. 1.

with an MD and MAD of −0.05 and 0.05 eV and a maximum absolute error of only 0.10 eV. The AHFC calculations again give higher-energy maxima (MD = +0.14 eV, MAD = 0.14 eV).

Taken together, these results indicate that a substantial part of the residual uncertainty in the calculated band maxima is associated with the spectral simulation treatment rather than with a uniform shift of the underlying electronic-state energies. This is evident from the frequent reversal of the signed deviations between the NEA and AHFC results: their mean deviations have opposite signs for five of the ten statistical subsets considered, and the two treatments bracket the experimental maxima for 42 of 83 directly comparable individual bands (51%). The magnitude of this effect is therefore comparable to, and in some subsets larger than, the residual deviation of the calculated band positions themselves.

A particularly striking result emerges for the directly resolved photobase L_b 0–0 transition energies. For the four neutral species for which a direct comparison between an experimental spectral origin and a calculated TBE is avail-

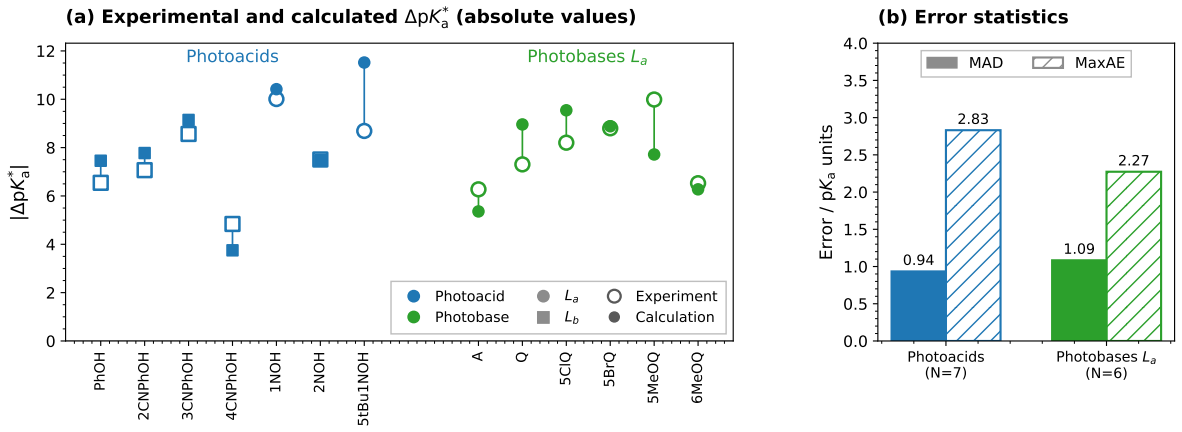


Figure 5. Experimental and calculated excited-state acidity/basicity changes, $-\Delta pK_a^*$ for photoacids and $+\Delta pK_a^*$ for photobases. The calculated values are derived from Wigner absorption–fluorescence midpoint 0–0 estimates for the photoacid and photobase L_a subsets. Panel (b) summarizes the corresponding mean absolute deviations (MAD) and maximum absolute errors (MaxAE), using the same class colors as in panel (a).

able, Tab. 1 gives an MD and MAD of only 0.02 eV and a maximum absolute error of 0.03 eV. The corresponding six cationic species show an MD of 0.02 eV, an MAD of 0.02 eV. These deviations are an order of magnitude smaller than the largest errors encountered for the simulated band maxima. The molecule-resolved signed deviations are shown in Fig. 4. For $5CNQH^+$ and QH^+, however, the experimental L_b 0–0 positions are among the least certain in the data set because of the overlapping spectral contributions and the associated deconvolution. For both species, the discrepancy with the TBE is smaller when the position of the corresponding feature in the original spectrum is used instead of the value obtained from the spectral fit. Thus, at least part of the comparatively large deviations for these two species likely reflects uncertainty in the experimental assignment. For most of the remaining species, the deviations amount to only approximately 0.01–0.02 eV, with AH^+ reproduced essentially exactly. Acridine provides the additional case for which an experimentally resolved L_a 0–0 origin is available; the corresponding deviation between the TBE and the experimental result of +0.02 eV is similarly small as for the L_b transition in this species. The complete state-resolved 0–0 energies and their errors are provided in the Supporting Information (Tab. S8 and Fig. S5).

Overall, the present framework reproduces most absorption and fluorescence band positions with an accuracy in the order of ±0.1–0.2 eV, while the directly resolved photobase L_b 0–0 transition energies reach a substantially higher accuracy of only a few hundredths of an eV.

From Spectroscopy to Excited-State Acid–Base Thermodynamics

The present set of photoacids and photobases has previously been used to benchmark the prediction of excited-state acidity and basicity in aqueous solution.[32,49] The central quantity is the change in acidity upon electronic excitation,

$$\Delta \mathrm{p}K_\mathrm{a}^* = \mathrm{p}K_\mathrm{a}^* - \mathrm{p}K_\mathrm{a} = \frac{\Delta E(\mathrm{base}) - \Delta E(\mathrm{acid})}{RT\ln(10)}, \quad (1)$$

where ΔE denotes the corresponding ground- to excited-state energy difference.[50,51] Because $\Delta \mathrm{p}K_\mathrm{a}^*$ is obtained from the difference between excitation energies of two protonation states, it provides a sensitive test for a balanced description of solvation effects in aqueous solution and of error cancellations: similar residual errors largely cancel, whereas errors of different magnitude or sign accumulate in the results for $\Delta \mathrm{p}K_\mathrm{a}^*$. The solvent-induced shifts of the vertical excitation energies depend strongly on the protonation state and on the electronic character of the transition, in particular its charge-transfer character (Tabs. S5 and S6, SI). For the photoacids, substantially larger shifts are found for the deprotonated forms than for the corresponding neutral species, while for the photobases pronounced protonation-dependent shifts occur particularly for the L_a states. This strong state and protonation dependence of the solvent response is therefore especially important for the accurate prediction of $\Delta \mathrm{p}K_\mathrm{a}^*$.

For a direct comparison with experiment, the following analysis employs 0–0 estimates derived from the absorption and fluorescence band maxima as:[2,32]

$$E_{00}^{\mathrm{mid}} = \frac{1}{2}\left(E_{\mathrm{max}}^{\mathrm{abs}} + E_{\mathrm{max}}^{\mathrm{em}}\right). \quad (2)$$

Experimental and calculated values are thus obtained on the same basis, with the calculated midpoints taken from the NEA spectra. The complete E_{00}^{mid} analysis and alternative results from the vibronic spectra are provided in the Supporting Information (Tabs. S7–S9, Figs. S4–S5).

The resulting $\Delta \mathrm{p}K_\mathrm{a}^*$ values are summarized in Fig. 5 (see Tabs. S10–S13 for further details). For the photoacids ($\Delta \mathrm{p}K_\mathrm{a}^* < 0$), seven systems provide complete and experimentally comparable acid–base cycles. Most of the calculated values agree very well with the values derived from the experimental spectra. An outlier is 5-*tert*-butyl-1-naphthol (5tBu1NOH) with exceptional large deviation. Here, the NEA result for the fluorescence band of the 5-*tert*-butyl-1-naphtholate anion underestimates the experimental band maximum by 0.43 eV and largely accounts for the ΔpK_a^* deviation of 2.83 units. This might be related to the fact that for 5tBu1NOH and $5tBu1NO^-$ we could optimize the ground- and excited-state geometries only with COSMO as solvation model, which doesn't properly describe solvation effects from hydrogen bonding, which are large for phenolate and naphtholate anions. The result for 5tBu1NOH is

additionally affected by uncertainties in the state assignments for the experimental absorption spectra of the neutral naphthol due to overlapping contributions from L_a and L_b, which could not be deconvoluted. The two cyano-naphthols for which no complete experimental absorption–fluorescence midpoint cycles are available have been excluded from the above analysis of $\Delta \mathrm{p}K_\mathrm{a}^*$.

Also, the hydroxycoumarins are not included in the above analysis because the corresponding experimental reference cycles are subject to additional uncertainties. For 3-hydroxycoumarin, a fixed neutral/anion absorption–fluorescence midpoint cycle can be defined, but the experimental spectra lead to a comparatively uncertain midpoint reference since the deconvolution of the absorption spectrum of 3-hydroxcoumarin lead to ambiguous results. For 7-hydroxycoumarin and 7-hydroxy-4-methylcoumarin, the coupled (de-)protonation equilibria between the normal and the tautomeric neutral and the anionic species complicate the assignment of directly comparable absorption and fluorescence contributions.

For the photobases ($\Delta \mathrm{p}K_\mathrm{a}^* > 0$), it is for all molecules in the test set the L_a state which is observed in emission and responsible for the photobasicity. Formal $\Delta \mathrm{p}K_\mathrm{a}^*$ values derived from the photobase L_b 0–0 energies are provided in the Supporting Information for completeness (Tabs. S12–S13). Complete midpoint-based cycles are available for six systems. The overall accuracy is similar as for the photoacids: the mean absolute deviation is 1.09 $\mathrm{p}K_\mathrm{a}$ units for the photobases and 0.94 units for the photoacids (Fig. 5(b)) and the maximum absolute deviations 2.27 and 2.83 units, respectively.

Thus, once the excitation energies are evaluated from the simulated absorption and fluorescence spectra, photoacidic and photobasic $\Delta \mathrm{p}K_\mathrm{a}^*$ values are reproduced with comparable accuracy. The remaining deviations reflect mostly how the residual deviations for the band maxima of the two protonation states cancel or accumulate when the corresponding energy differences are formed.

Conclusion

We have shown that state-specific EC-RISM-CC calculations with the PTED coupling scheme, employing CC2 for structure optimizations and frequencies and CC3 for energies, and combined with complementary NEA and AHFC methods for spectra simulations, provide accurate band maxima for absorption and fluorescence spectra in aqueous solution without empirical adjustment of the spectral positions. The computational costs for this workflow are compatible with its application in routine calculations. Across the photoacid and photobase benchmark sets, the calculated band maxima are typically reproduced within approximately 0.1–0.2 eV and the directly resolved photobase L_b 0–0 transition energies reach a substantially higher accuracy of only a few hundredths of an eV. At the same time, the comparison between NEA and AHFC spectra shows that the remaining deviations of the band maxima are not governed solely by the underlying electronic-state energies. The frequent reversal of the signed errors between the two spectral treatments demonstrates that the approximations used to describe the nuclear distribution and vibronic band structure constitute an important part of the residual uncertainty. For many cases the absorption bands for L_a and L_b overlap and the deconvolution of the experimental spectrum into separate contributions from the two states causes also an uncertainties in the data for the experimental band maxima.

Beyond the overall spectral positions, the state-specific treatment provides access to the electronic-state composition and photochemical origin of the observed spectra. This includes the resolution of L_a and L_b contributions in the photobases, and cases in which state reordering between vertical and 0–0 transitions or tautomerization change the state or molecular form responsible for absorption and fluorescence. The same computational framework can therefore describe a chemically diverse set of aqueous excited-state processes rather than only isolated transition energies including excited-state acidity and basicity changes without empirical correction. For the systems with complete experimental spectral cycles, the mean absolute deviations of $\Delta \mathrm{p}K_\mathrm{a}^*$ are 1.25 and 1.09 units for the photoacids and photobases, respectively. The remaining errors are determined primarily by whether the residual excitation-energy deviations of the corresponding protonation states cancel or accumulate when the thermodynamic energy differences are formed. Taken together, these results establish the combination of EC-RISM with coupled-cluster methods and the state-specific self-consistent PTED(LR) coupling scheme as a route to accurate ground- and excited-state electronic structure calculations in aqueous solution including systems where solvation and charge transfer contributions are large.

Acknowledgements

We thank the Deutsche Forschungsgemeinschaft (DFG, German Research Foundation) for funding under Germany's Excellence Strategy–EXC 2033–390677874–RESOLV.

Conflict of Interest

Please enter any conflict of interest to declare.

Data Availability Statement

The original data such as input and output files for the the electronic structure calculations and spectra simulations, spreadsheets with compiled data and digitalized spectra, and scripts used to analyze the data and prepare tables and figures for the main text and the Supporting Information are available from RESOLVdata[52] at https://doi.org/10.17877/RESOLV-2026-MULD5A7K_2026.

Keywords: Absorption and fluorescence spectroscopy • Coupled-cluster theory • EC-RISM solvation • Photoacids and photobases • Excited-state proton transfer

References

[1] T. J. Zuehlsdorff, S. V. Shedge, S.-Y. Lu, H. Hong, V. P. Aguirre, L. Shi, C. M. Isborn, *Annu. Rev. Phys. Chem.* **2021**, *72*, 165.

[2] F. J. Avila Ferrer, J. Cerezo, E. Stendardo, R. Improta, F. Santoro, *J. Chem. Theory Comput.* **2013**, *9*, 2072.

[3] F. Santoro, R. Improta, A. Lami, J. Bloino, V. Barone, *J. Chem. Phys.* **2007**, *126*, 084509.

[4] A. Baiardi, J. Bloino, V. Barone, *J. Chem. Theory Comput.* **2013**, *9*, 4097.

[5] F. J. Avila Ferrer, J. Cerezo, J. Soto, R. Improta, F. Santoro, *Comput. Theor. Chem.* **2014**, *1040–1041*, 328.

[6] S. V. Shedge, T. J. Zuehlsdorff, A. Khanna, S. Conley, C. M. Isborn, *J. Chem. Phys.* **2021**, *154*, 084116.

[7] A. Petrone, J. Cerezo, F. J. Avila Ferrer, G. Donati, R. Improta, N. Rega, F. Santoro, *J. Phys. Chem. A* **2015**, *119*, 5426.

[8] T. J. Zuehlsdorff, C. M. Isborn, *J. Chem. Phys.* **2018**, *148*, 024110.

[9] T. J. Zuehlsdorff, C. M. Isborn, *Int. J. Quantum Chem.* **2019**, *119*, e25719.

[10] L. E. de Sousa, P. de Silva, *J. Phys. Chem. A* **2023**, *127*, 8200.

[11] M. S. Chen, Y. Mao, A. Snider, P. Gupta, A. Montoya-Castillo, T. J. Zuehlsdorff, C. M. Isborn, T. E. Markland, *J. Phys. Chem. Lett.* **2023**, *14*, 6610.

[12] S. Abou-Hatab, V. Carnevale, S. Matsika, *J. Chem. Phys.* **2021**, *154*, 064104.

[13] A. Khanna, S. V. Shedge, T. J. Zuehlsdorff, C. M. Isborn, *J. Chem. Phys.* **2024**, *161*, 044121.

[14] S. Tsuru, B. Sharma, C. Hättig, D. Marx, *Angew. Chem. Int. Ed.* **2025**, *64*, e202416058.

[15] F. Mazza, M. Trinari, C. Sepali, C. Cappelli, *J. Chem. Theory Comput.* **2026**, *22*, 1350.

[16] A. Snider, M. S. Chen, T. E. Markland, C. M. Isborn, *J. Chem. Phys.* **2026**, *164*, 134102.

[17] D. Bashirova, J. Stein, K. Siegfried, T. J. Zuehlsdorff, *J. Chem. Phys.* **2026**, *164*, 174308.

[18] H. Moumene, G. Prampolini, C. García-Iriepa, J. Cerezo, I. Navizet, F. Santoro, *J. Phys. Chem. B* **2025**, *129*, 2829.

[19] B. Lunkenheimer, A. Köhn, *J. Chem. Theory Comput.* **2013**, *9*, 977.

[20] C. Hättig, A. Pausch, *J. Phys. Chem. A* **2025**, *129*, 6155.

[21] K. Kanemaru, T. Yamaguchi, N. Yoshida, H. Sato, *Phys. Chem. Chem. Phys.* **2026**, *28*, 18311.

[22] T. Kloss, J. Heil, S. M. Kast, *J. Phys. Chem. B* **2008**, *112*, 4337.

[23] S. M. Kast, T. Kloss, *J. Chem. Phys.* **2008**, *129*, 236101.

[24] J. Haberhauer, P. Kibies, S. M. Kast, C. Hättig, *J. Chem. Theory Comput.* **2026**, *22*, 6742.

[25] O. Christiansen, H. Koch, P. Jørgensen, *Chem. Phys. Lett.* **1995**, *243*, 409.

[26] A. Klamt, G. Schüürmann, *J. Chem. Soc., Perkin Trans. 2* **1993**, pages 799–805.

[27] A. Klamt, *WIREs Comput. Mol. Sci.* **2018**, *8*, e1338.

[28] N. Sülzner, G. Jung, P. Nuernberger, *Chem. Sci.* **2025**, *16*, 1560.

[29] A. Yucknovsky, N. Amdursky, *Angew. Chem. Int. Ed.* **2025**, *64*, e202422963.

[30] J. Valdez, M. Warner, C. Ramos, V. Silva, D. Varasteh, S. del Pozo, S. Pecic, J. R. Hunt, A. S. Petit, *J. Phys. Org. Chem.* **2026**, *39*, e70101.

[31] M. A. Hernandez Vieyra, T. J. Megna, S. Angulo, A. S. Petit, *J. Phys. Chem. A* **2026**, *130*, 2016.

[32] Ö. F. C. Tiska, N. Sülzner, J. Haberhauer, P. Kibies, S. M. Kast, C. Hättig, *Phys. Chem. Chem. Phys.* **2025**, *27*, 17930.

[33] H. Koch, O. Christiansen, P. Jørgensen, A. M. Sánchez de Merás, T. Helgaker, *J. Chem. Phys.* **1997**, *106*, 1808.

[34] R. Crespo-Otero, M. Barbatti, *Theor. Chem. Acc.* **2012**, *131*, 1237.

[35] J. R. Platt, *J. Chem. Phys.* **1949**, *17*, 484.

[36] K. M. Solntsev, D. Huppert, N. Agmon, *J. Phys. Chem. A* **1998**, *102*, 9599.

[37] E. Pines, UV-Visible Spectra and Photoacidity of Phenols, Naphthols and Pyrenols, in Z. Rappoport (Editor), *The Chemistry of Phenols*, pages 491–527, John Wiley & Sons, Chichester **2003**.

[38] J. R. Hunt, C. Tseng, J. M. Dawlaty, *Faraday Discuss.* **2019**, *216*, 252.

[39] S. Kundu, P. P. Roy, G. R. Fleming, N. Makri, *J. Phys. Chem. B* **2022**, *126*, 2899.

[40] S. Kaneko, S. Yotoriyama, H. Koda, S. Tobita, *J. Phys. Chem. A* **2009**, *113*, 3021.

[41] R. Knochenmuss, P. L. Muiño, C. Wickleder, *J. Phys. Chem.* **1996**, *100*, 11218.

[42] D. Xiao, M. Prémont-Schwarz, E. T. J. Nibbering, V. S. Batista, *J. Phys. Chem. A* **2012**, *116*, 2775.

[43] F. Messina, M. Prémont-Schwarz, O. Bräm, D. Xiao, V. S. Batista, E. T. J. Nibbering, M. Chergui, *Angew. Chem. Int. Ed.* **2013**, *52*, 6871.

[44] L. M. Tolbert, J. E. Haubrich, *J. Am. Chem. Soc.* **1990**, *112*, 8163.

[45] T. Moriya, *Bull. Chem. Soc. Jpn.* **1983**, *56*, 6.

[46] T. Moriya, *Bull. Chem. Soc. Jpn.* **1988**, *61*, 1873.

[47] E. A. Routsi, M. A. Theodoropoulou, C. Mantzourani, D. Tzeli, C. G. Kokotos, G. Kokotos, *ChemCatChem* **2026**, *18*, e71065.

[48] E. W. Driscoll, J. R. Hunt, J. M. Dawlaty, *J. Phys. Chem. Lett.* **2016**, *7*, 2093.

[49] A. Ghiami-Shomami, C. Hättig, *J. Comput. Chem.* **2023**, *44*, 1941.

[50] T. Förster, *Naturwissenschaften* **1949**, *36*, 186.

[51] T. Förster, *Z. Elektrochem. Angew. Phys. Chem.* **1950**, *54*, 42.

[52] C. Hättig, N. Sülzner, Replication Data for: "Absorption and Emission Spectra in Aqueous Solution with Coupled-Cluster Accuracy" **2026**.